⌘ *Author's Choice*

THE JOURNAL OF BIOLOGICAL CHEMISTRY VOL. 287, NO. 46, pp. 38637–38646, November 9, 2012
Published in the U.S.A.

Dynamic Exchange of Myosin VI on Endocytic Structures*[S]

Received for publication, April 23, 2012, and in revised form, September 11, 2012 Published, JBC Papers in Press, September 19, 2012, DOI 10.1074/jbc.M112.373969

Lisa M. Bond[‡§], Susan D. Arden[§], John Kendrick-Jones[¶], Folma Buss[§1], and James R. Sellers[‡2]

From the [‡]Laboratory of Molecular Physiology, NHLBI, National Institutes of Health, Bethesda, Maryland 20892 , the [§]Cambridge Institute for Medical Research, University of Cambridge, Wellcome Trust/Medical Research Council Building, Hills Road, Cambridge CB2 0XY, United Kingdom; and the [¶]Medical Research Council Laboratory of Molecular Biology, Hills Road, Cambridge CB2 2QH,United Kingdom

Background: Myosin VI turnover during endocytosis is underexplored.
Results: Wild type myosin VI exchanges at the same rate as its binding partner and faster than artificially dimerized myosin VI.
Conclusion: During endocytic exchange, myosin VI relies on binding partner dynamics and does not function as a stable dimer.
Significance: The turnover dynamics and monomer/dimer properties of myosin VI are illuminated.

The actin-based molecular motor myosin VI functions in the endocytic uptake pathway, both during the early stages of clathrin-mediated uptake and in later transport to/from early endosomes. This study uses fluorescence recovery after photobleaching (FRAP) to examine the turnover rate of myosin VI during endocytosis. The results demonstrate that myosin VI turns over dynamically on endocytic structures with a characteristic half-life common to both the large insert isoform of myosin VI on clathrin-coated structures and the no-insert isoform on early endosomes. This half-life is shared by the myosin VI-binding partner Dab2 and is identical for full-length myosin VI and the cargo-binding tail region. The 4-fold slower half-life of an artificially dimerized construct of myosin VI on clathrin-coated structures suggests that wild type myosin VI does not function as a stable dimer, but either as a monomer or in a monomer/dimer equilibrium. Taken together, these FRAP results offer insight into both the basic turnover dynamics and the monomer/dimer nature of myosin VI.

The myosins in class VI are distinguished in their role as intracellular motor proteins by their unique ability to move toward the minus end of actin filaments (1). This directional bias, determined by the presence of a 53-amino acid insert (reverse gear) proximal to the motor domain (2), renders myosin VI a critical functional component of several, direction-specific intracellular processes. For example, in the secretory pathway, myosin VI maintains Golgi complex morphology (3) and is required for the sorting of cargo to the leading edge of motile cells (4) and to the basolateral domain of polarized epithelial cells (5). In this pathway, myosin VI has also been shown to modulate the fusion of secretory vesicles with the plasma membrane during the final stages of exocytosis (6).

Myosin VI has also been broadly implicated in endocytosis, the critical cellular pathway by which essential proteins and nutrients are transferred from the external environment to the interior of a cell. The mammalian myosin VI isoform with a 21–31-amino acid "large insert" (LI)[3] just before the C-terminal cargo-binding portion of the tail domain (7) is specifically linked with the early stages of the clathrin-mediated endocytic pathway, a subcategory of endocytosis involving uptake into pits and vesicles coated with the protein clathrin ("clathrin-coated structures"). This myosin VI LI splice variant is selectively expressed in polarized epithelial cells, where it co-localizes at the apical domain with clathrin-coated structures (7) and has been shown by total internal reflection fluorescence microscopy to be actively recruited to clathrin-coated structures (8). Studies from the myosin VI KO mouse, the Snell's waltzer mouse, have demonstrated that myosin VI is essential for cystic fibrosis transmembrane conductance regulator endocytosis in enterocytes (9), as well as for the endocytic uptake of α-amino-3-hydroxy-5-methyl-4-isoxazole propionic acid-type glutamate receptors (AMPARs) in hippocampal neurons (10). Myosin VI is also involved in the later stages of endocytosis. The myosin VI no insert (NI) isoform has been implicated in the transport of uncoated endocytic vesicles through the cortical actin network to early endosomes (11) and is required for the sorting of cargo at early endosomes and the delivery of cargo from early endosomes to endocytic recycling compartments (12, 13).

It is crucial to understand the specifics of these varied functional roles for myosin VI, as abnormalities in myosin VI function have been linked to such diseases as prostate and ovarian cancer (14, 15), hypertrophic cardiomyopathy (16), neurodegeneration (10), and deafness (17–19). Perhaps the most critical target for such directed studies of myosin VI function is the well established role for myosin VI in the vesicle transport processes

* This work was supported, in whole or in part, by the NHLBI, National Institutes of Health, Intramural Program (to J. R. S.). This work was also supported by the Wellcome Trust (to F. B.), a scholarship from the Winston Churchill Foundation of the United States (to L. M. B.), a National Institutes of Health-Oxford-Cambridge Ph.D. studentship (to L. M. B.), and the Medical Research Council (to J. K-J.). The Cambridge Institute for Medical Research received a strategic award from the Wellcome Trust.
⌘ *Author's Choice*—Final version full access.
[S] This article contains supplemental Table 1 and Fig. 1.
[1] To whom correspondence may be addressed. Tel.: 44-0-1223-763348 (office) or 44-0-1223-336782 (laboratory); Fax: 44-0-1223-762640; E-mail: fb1@mole.bio.cam.ac.uk.
[2] To whom correspondence may be addressed: NHLBI, National Institutes of Health, 50 South Dr., Bldg. 50, Rm. 3523, Bethesda, MD 20892. Tel.: 1-301-496-6887; E-mail: sellersj@nhlbi.nih.gov.

[3] The abbreviations used are: LI, large insert; AA, amino acid(s); CCS, clathrin-coated structure; FRAP, fluorescence recovery after photobleaching; NI, no insert; RPE, retinal pigment epithelial.

of the endocytic uptake pathway, as it is likely that this function makes a major contribution to the motor disease involvement. For example, defects in myosin VI-driven endocytic membrane transport processes in stereocilia may cause deafness, absence of myosin VI causes accumulation of cystic fibrosis transmembrane conductance regulator in enterocytes leading to secretory diarrhea, and the lack of endocytosis of specific glutamate receptors in myosin VI-depleted cells may result in neurodegeneration (7, 10, 20). Thus, a thorough understanding of the roles of myosin VI in endocytosis is critical for identifying the endocytic malfunctions that may cause specific diseases and the subsequent development of new targeted treatments to correct these malfunctions.

Although some of the features of myosin VI involvement in endocytosis are known (*e.g.* the binding partners involved), the specifics of its function on this pathway still require direct investigation. It has been suggested that the myosin VI LI isoform in polarized epithelial cells plays a role in the clustering of cell surface receptors into a clathrin-coated pit, in the formation of clathrin-coated vesicles, and in clathrin-coated vesicle transport away from the plasma membrane (21, 22), but no studies have so far demonstrated directly whether the myosin VI LI isoform plays a short or long term role in such tethering/transport processes or investigated the turnover kinetics of its association with clathrin-coated structures. On a more fundamental level, it is not clear whether myosin VI functions in endocytosis as a monomer or a dimer, a question of great importance in the field given the widespread dissent as to whether myosin VI has a natural tendency toward self-dimerization (23, 24). In particular, it has not been addressed whether myosin VI might transfer dynamically between an inactive, folded, monomeric conformation in the cytosol (comparable with that of myosin VII) (25, 26) and an active, unfolded, dimeric conformation (*e.g.* when actively bound via Dab2 to clathrin-coated vesicles) (24, 27, 28).

In this study, we investigate the specifics of the dynamic association of myosin VI with clathrin-coated structures and early endosomes using the microscopic method of fluorescence recovery after photobleaching (FRAP). As an initial probe into the basic kinetics of myosin VI involvement in endocytosis, we demonstrate the dynamic exchange and characteristic half-life of the myosin VI NI isoform on early endosomes and myosin VI LI isoform on clathrin-coated structures. We then demonstrate that the characteristic half-life of myosin VI is shared by Dab2, the binding partner known to recruit myosin VI to clathrin-coated structures. Our FRAP assay is then used to examine the turnover dynamics of myosin VI mutant constructs, a means of gaining insight into the behavior of myosin VI on the endocytic pathway. The results indicate that myosin VI is likely to behave as a functional monomer or as a dynamic monomer/dimer during endocytosis, because a novel artificial dimer construct of myosin VI designed for live cell expression displays strikingly different turnover dynamics from wild type myosin VI. The observation that a tail construct of myosin VI turns over at the same rate as the full-length molecule targets the tail domain as a critical determinant of turnover dynamics. Taken together, these results provide insight into the dynamics and monomer/dimer nature of myosin VI during endocytosis.

EXPERIMENTAL PROCEDURES

Antibodies—The following primary antibodies were used: rabbit polyclonal antibody to GFP (Invitrogen); mouse monoclonal antibody to clathrin (Abcam); mouse monoclonal antibody to Rab5 (BD Biosciences).

Cell Culture and Transfection—The HeLa cell line used in this study was maintained at 37 °C in Dulbecco's modified Eagle's medium (DMEM; Invitrogen) supplemented with 10% fetal calf serum (FCS) (Sigma-Aldrich), 2 mM L-glutamine, and penicillin/streptomycin (Sigma-Aldrich). Retinal pigment epithelial (RPE) cells were maintained at 37 °C in a 1:1 mixture of DMEM and Ham's Nutrient Mixture F-12 (Invitrogen), supplemented with 10% FCS, 2 mM L-glutamine, penicillin/streptomycin, and 2% sodium bicarbonate (Invitrogen). Chinese Hamster Ovary (CHO) cells were maintained at 37 °C in Ham's Nutrient Mixture F-12, supplemented with 10% FCS, 2 mM L-glutamine, and penicillin/streptomycin.

Transfection of the plasmids into tissue culture cells was executed according to the instructions provided by the manufacturer of the FuGENE transfection reagent (Roche Diagnostics). Before transfection, cells were grown to 50% confluence on a 6-well tissue culture tray (Greiner Bio-One). Unless otherwise specified, 2 μg of plasmid DNA and 6 μl of FuGENE transfection reagent diluted in 95 μl of OptiMEM I (Invitrogen) were used for each given transfection in 1 well of the 6-well tray.

Immunofluorescence—Cells for use in immunofluorescence experiments were grown overnight on square coverslips placed in 6-well trays. Coverslips were then incubated in 0.05% saponin in phosphate-buffered saline (PBS) for 30 s before fixing with 4% paraformaldehyde in PBS for 20 min, permeabilized in 0.2% Triton X-100 in PBS for 5 min, quenched with 10 mM glycine in PBS for 15 min, and blocked in 1% BSA in PBS for 30 min. After blocking, coverslips were incubated for 1 h in primary antibodies, washed with PBS for three 5-min intervals, incubated for 1 h in the appropriate secondary antibodies, and then washed with PBS in five 5-min intervals. The coverslips were then mounted on glass slides (Agar Scientific) with Prolong Gold Antifade Mounting Reagent (Molecular Probes).

Myosin VI Leucine Zipper Construct for in Vivo Expression—The artificially dimerized form of myosin VI used in many *in vitro* studies over the last 10 years consists of a form of porcine myosin VI truncated in the tail domain after amino acid 992 and containing a C-terminal GCN4 leucine zipper sequence (MKQLEDKVEELLSKNYHLENEVARLKKLVGER) (29, 30). We designed a unique, full-length form of large insert, human myosin VI with the same GCN4 leucine zipper sequence (designed to follow a human codon bias) placed as an insert after the corresponding human amino acid 991 (GenScript). This version of the artificial dimer is distinguished by its capacity for live cell expression, as it retains the targeting regions in the myosin VI tail domain.

Plasmids Used for in Vivo Expression—The constructs used in this work were subcloned into mammalian expression vectors for transfection into HeLa or RPE cells. Full-length wild type myosin VI LI, wild type myosin VI, and the tail construct of myosin VI LI (excluding the first 838 N-terminal amino acids of the myosin VI protein) were each subcloned into the XhoI/

SacII sites of a pEGFP-C3 vector (Clontech). Dab2 was subcloned into the EcoRI/SalI sites of a pEGFP-C2 vector (Clontech). The full-length myosin VI LI leucine zipper construct was subcloned into the BamHI/ApaI sites of a pEGFP-C3 vector, and the myosin VI leucine zipper tail construct (similarly excluding the first 838 N-terminal amino acids of the myosin VI protein) was subcloned into the XhoI/SalI sites of a pEGFPC3 vector. pEGFPC3-clathrin was kindly provided by Prof. Margaret Robinson (Cambridge Institute for Medical Research).

Mammalian Two-hybrid Assay—The mammalian two-hybrid assay was conducted as described in a previous study from our laboratory (33). In short, three myosin VI "bait" constructs ((i) myosin VI LI globular tail (wild type AA 1030–1285); (ii) myosin VI LI globular tail + leucine zipper (AA 991–1317 of myosin VI LI leucine zipper construct described above); (iii) myosin VI LI globular tail with WWY→WLY mutation (wild type AA 1030–1285)) were cloned into a pM bait vector coding for the DNA-binding domain of the GAL4 transcription factor (Clontech). Dab2 (AA 550–770) was cloned into a pV16 "prey" vector coding for an activating domain derived from herpes simplex virus type 1 (Clontech). These bait and prey vectors were then co-transfected into CHO cells with a reporter plasmid coding for constitutively expressed *Renilla* luciferase (pRL-CMV; Promega Corp.) and a GAL4-inducible reporter plasmid coding for firefly luciferase expression (pG5*luc*; Promega) (0.5 μg each). CHO cells were grown for 48 h, lysed in a Passive Lysis buffer (Promega), and assayed for *Renilla* and firefly luciferase with a Dual-Luciferase Reporter Assay system (Promega). As a negative control, background luciferase activity was measured in cells transfected with pRL-CMV, pG5*luc*, Dab2/pV16, and an empty pM vector. Luciferase activity for each construct was calculated as the ratio of firefly to *Renilla* activity for that construct divided by the ratio of firefly to *Renilla* activity for the negative control.

FRAP Microscopy Assay—FRAP experiments were carried out on a Zeiss LSM 510 Incubated Confocal Microscope (Carl Zeiss, Inc.) with a heated stage and a Plan-Apochromat 63× lens. Images were acquired using LSM 510 acquisition software (Carl Zeiss, Inc.). Cells were incubated at 37 °C during acquisition.

During each FRAP experiment, a specific 40 × 40-pixel region at the cell base containing fluorescent constructs of interest was selected for study. Five single-scanned images of the entire cell containing this region were acquired. The region was then photobleached with 75 successive scans with a 488-nm argon laser line. Images of the entire cell were again acquired for the 2.5 min following bleaching. After image acquisition was complete, the Zeiss LSM 510 software was used to record the fluorescence intensity (arbitrary units) at each time point of both the bleached region and an unbleached reference region of the same dimensions and similar fluorescence level in an adjacent cell.

The FRAP data sets for each construct consisted of between 5 and 11 HeLa or RPE cells transfected with the construct of interest. Each FRAP study utilized between 4 and 6 individual sets of this type. Thus, no FRAP results are presented for which <4 data sets of at least 5 cells each were analyzed.

Quantification of Half-life ($t_{1/2}$) Values from FRAP Data—Analysis of FRAP photobleaching experiments was conducted by using Microsoft Excel and OriginPro to evaluate intensity data exported from Zeiss LSM imaging software. To correct the fluorescence intensities in the 40 × 40-pixel bleached region for photobleaching due to image acquisition, the intensities at each time point were multiplied by the inverse of the fluorescence intensity of an unbleached, 40 × 40-pixel reference region with a similar concentration of fluorescent structures in a nearby control cell. The resulting, corrected intensity values were used in the half-life calculations described below.

All FRAP analysis was conducted with the traditional representation of a given exchange/turnover process as a pseudo-first-order reaction. To confirm the validity of such analysis for our particular system, we quantified the relative levels of a representative fluorescent myosin VI construct (myosin VI LI) on endocytic structures *versus* in the surrounding cytoplasm. We found that levels of this representative construct are in significant excess in the cytoplasm *versus* on endocytic structures (50 ± 30-fold (±S.D.) higher concentration in the cytoplasm; $p = 6 \times 10^{-10}$). This significant cytoplasmic surplus indicates that the rate-limiting factor in a given exchange reaction is the first-order reaction of construct dissociation from endocytic structures. As such, FRAP exchange reactions can reasonably be analyzed as pseudo-first-order reactions for any given cell and should not be affected by relative construct expression levels. For reference, however, we have provided the overall expression levels of each construct analyzed (supplemental Table 1).

The half-life and percentage recovery were calculated for dynamic proteins in a manner comparable with the methods of a previous study (31). Prior to calculation, all images were corrected for photobleaching (as described above), normalized to a starting value of 1, and converted to real-time values (with prebleach as a negative time value, post-bleach as 0 s, and all subsequent images increasing in time from this zero point). The half-life was determined by fitting a single exponential to a plot of fluorescence in the experimental region *versus* real time in OriginPro. The percentage of fluorescence recovery was calculated from the asymptote provided by this single exponential fit.

Analysis of Expression Levels—The overall expression level of each construct was quantified by calculating the average total fluorescent intensity (arbitrary intensity units) at the base of 15 independent cells expressing the relevant construct (supplemental Table 1). Images for this analysis were acquired on a Zeiss LSM microscope with a 63× oil lens. Intensity levels were analyzed using Volocity Analysis software (PerkinElmer Life Sciences).

The ratio of cytoplasmic *versus* clathrin-coated structure-bound fluorescent constructs was determined using a reference examination of large insert myosin VI in HeLa cells. For these studies, a Zeiss LSM 510 microscope with a 63× oil lens was used to collect Z-stack images of 15 independent HeLa cells expressing eGFP-tagged myosin VI LI. In accordance with the Nyquist-Shannon sampling theorem, images were acquired at 0.5-μm intervals from the cell base to the top of the cell.

MetaMorph imaging software (Molecular Devices) was then used to calculate the sum of the fluorescent construct intensity

on punctate, clathrin-coated structures *versus* the surrounding cytoplasm for each slice of each Z-stack. Intensity levels for these regions were summed for each slice of a given cell to find the total sum of clathrin-associated *versus* cytoplasmic myosin VI LI fluorescence in each cell. The ratios of cytoplasmic to clathrin-coated structure-bound myosin VI for each cell were then calculated and averaged to demonstrate the significant cytoplasmic excess of this representative fluorescent construct.

Image Processing—Individual images were processed in Adobe Photoshop, and figures were assembled in Adobe Illustrator.

RESULTS

In this study, we used a FRAP assay to examine the lifetime and dynamics of myosin VI on endocytic structures. After first probing the basics of the turnover of myosin VI isoforms on clathrin-coated structures and early endosomes, we applied our assay to an investigation of the dynamic behavior of myosin VI variants in the endocytic pathway.

The LI and NI Isoforms of Myosin VI Turn Over Dynamically on Endocytic Structures with the Same Characteristic Half-life—We began our examination of myosin VI during endocytosis by using FRAP to examine the dynamics of two different myosin VI isoforms on the specific endocytic structures to which they are recruited.

The localization of the large insert isoform of myosin VI to clathrin-coated structures (CCSs) has been well established. For example, endogenous large insert myosin VI has been shown to localize to clathrin-coated vesicles in the apical domain of polarized Caco-2 cells (7). Although the large insert isoform of myosin VI is not endogenously expressed in HeLa cells, fluorescently tagged myosin VI LI-eGFP constructs localize to clathrin-coated structures at the plasma membrane of HeLa cells in a manner similar to the endogenous LI isoform in other cell lines (Fig. 1*A*, *a–c*) (7). As such, the robust and easy to handle HeLa cell line has previously been used as a system for the examination of myosin VI LI on clathrin-coated structures (32) and was used in this study to examine the dynamic behavior of large insert myosin VI. The recruitment of myosin VI LI to clathrin-coated pits/vesicles in this system produces characteristic small, round punctae at the plasma membrane that are easy to identify and select for photobleaching experiments (Fig. 1*A*, *a–c*).

The NI isoform of myosin VI is endogenously expressed in HeLa and RPE cells, and the functions of this isoform in endocytosis have been previously probed by expressing this isoform in RPE cells and studying its targeting to early endosomes (13, 32). After confirming the localization of eGFP-tagged myosin VI NI to early endosomes labeled with the characteristic marker protein Rab5 (Fig. 1*A*, *d–f*), we used the RPE cell line to examine the dynamic behavior of myosin VI NI. As is evident from the lower panel of Fig. 1*A*, the recruitment of myosin VI NI to early endosomes similarly produces a characteristic phenotype of round punctae in the cortical actin network beneath the plasma membrane that are easy to identify and select for photobleaching experiments.

We used a traditional FRAP imaging process to examine the turnover of myosin VI on clathrin-coated structures or early endosomes (Fig. 1*B*). For example, prior to bleaching (pre-bleach), myosin VI LI-eGFP constructs were localized to punctate clathrin-coated structures near the plasma membrane at the base of a HeLa cell (Fig. 1*Ba*). After targeted bleaching of a selected region of interest (post-bleach), the fluorescence intensity of the myosin VI LI on the multiple clathrin-coated structures within this region was extinguished (Fig. 1*Bb*). Monitoring this experimental region for the 2.5-min period after bleaching revealed that our FRAP system was sensitive enough to observe the dynamic replacement of bleached constructs on clathrin-coated structures in the experimental region with unbleached, fluorescent constructs from the surrounding area (Fig. 1*Bc*).

To analyze these FRAP data, the fluorescence intensities in specific regions of interest from each cell were corrected for photobleaching, averaged in sets of 5–9 cells, and plotted *versus* time to produce a recovery curve for a given set. The recovery curves were fit to a single exponential equation to determine the half-life ($t_{½}$) of this turnover process for each protein, which represents the time required for half of the construct fluorescence that will eventually recover to a given region to return to that region. Average half-lives for each construct were calculated from 4–5 sets of 5–9 individual cells.

Recovery curves were plotted for the data sets used to analyze the dynamic turnover of myosin VI LI-eGFP on clathrin-coated structures in HeLa cells and for myosin VI NI-eGFP on early endosomes in RPE cells (Fig. 1*C*). These plots take on the characteristic drop-and-gradual-rise shape of dynamic proteins, indicating that both isoforms of myosin VI turn over dynamically on endocytic structures. Comparison of the quantified half-lives of each isoform reveals that myosin VI NI has the same characteristic half-life on early endosomes in RPE cells ($t_{½} = 16 \pm 1$ s) as myosin VI LI on clathrin-coated structures in HeLa cells ($t_{½} = 13 \pm 2$ s) ($p = 0.3$) (Fig. 1*D*). Fig. 1*E* provides a line diagram comparison of these wild type myosin VI full-length LI and NI constructs with the truncated and mutant myosin VI constructs utilized in the ensuing subsections of this study.

Comparison with Other Members of the Endocytic Machinery: Myosin VI-binding Partner Dab2 Turns Over on Clathrin-coated Structures at the Same Rate as Myosin VI LI; Clathrin Has a 2-Fold Longer Half-life Than Wild Type Myosin VI LI—We next applied the robust system of analyzing turnover on clathrin-coated vesicles in HeLa cells to the comparative investigation of the turnover rates of two related proteins on the endocytic pathway: the myosin VI-binding partner Dab2 and the coat protein clathrin.

Dab2 binds to myosin VI and to the coat protein clathrin and has been shown to actively recruit myosin VI to clathrin-coated vesicles during endocytosis (32, 33). In fact, forms of myosin VI containing mutations in the WWY region of the tail domain to which Dab2 binds no longer associate with clathrin and so do not display their characteristic punctate, clathrin-coated structure-associated expression patterns at the cell surface (32). FRAP of the turnover of Dab2 on clathrin-coated structures in HeLa cells reveals that Dab2 turns over dynamically with a half-life of 10 ± 1 s, which is very similar to the half-life of myosin VI LI ($t_{½} = 13 \pm 2$ s) ($p = 0.2$) (Fig. 2, *A* and *C*).

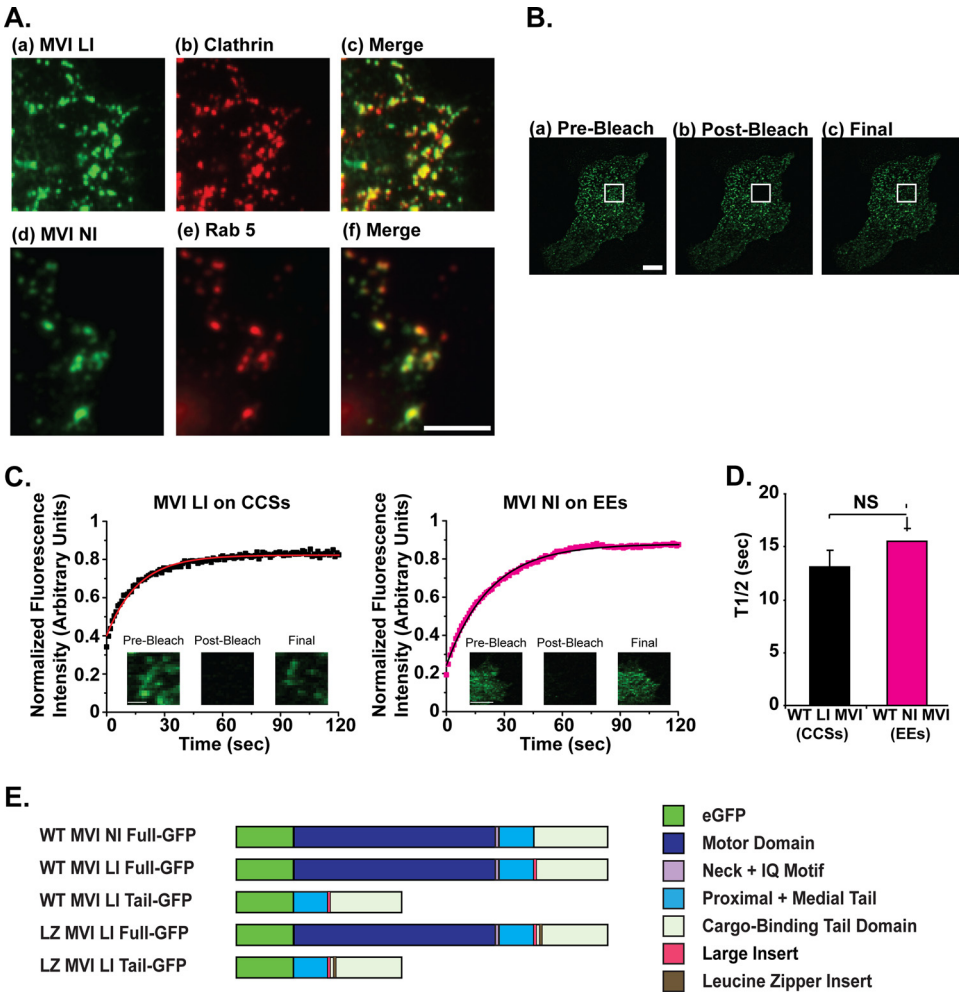

FIGURE 1. **The LI and NI isoforms of myosin VI turn over dynamically on endocytic structures with the same half-life.** *A*, myosin VI LI co-localizes with clathrin-coated structures in HeLa cells. *a–c*, sample images at the base of a HeLa cell transfected with eGFP-tagged myosin VI LI (*a*) and labeled in *red* for endogenous clathrin (*b*) demonstrate co-localization between myosin VI LI and the clathrin-coated pits/vesicles at the plasma membrane (*c*). Cells were labeled by immunofluorescence with a polyclonal antibody to eGFP and a monoclonal antibody to clathrin. Myosin VI NI co-localizes with early endosomes. *d–f*, sample images at the base of an RPE cell transfected with eGFP-tagged myosin VI NI (*d*) and labeled in *red* for the endogenous early endosome marker Rab5 (*e*) demonstrate co-localization between myosin VI NI and early endosomes at the plasma membrane (*f*). *Scale bar*, 2.5 μm. *B*, FRAP methodology. *a*, pre-bleach: at the start of imaging, the myosin VI is localized to punctate, clathrin-coated structures at the base of a HeLa cell. *b*, post-bleach: the fluorescence intensity of myosin VI proteins within the region of interest (*marked* with a *white square*) has been depleted by targeted bleaching with a high intensity laser line. *c*, final: within the 2.5-min imaging period, the bleached myosin VI proteins in the region of interest dissociate from clathrin-coated structures and are dynamically replaced by fluorescent myosin VI proteins from unbleached regions. *Scale bar*, 50 μm. *C*, FRAP of MVI LI on clathrin-coated structures in HeLa cells and MVI NI on early endosomes in RPE cells is shown. Each *plot* represents an average of 1 data set (5 individual cells (myosin VI NI) or 9 individual cells (myosin VI LI)); all intensity values were corrected for photobleaching due to image acquisition and normalized to a starting value of 1 before plotting. The *solid line* in each *plot* represents a single exponential fit to the data ($R^2 = 0.97$ for LI, 0.99 for NI). Representative pre-bleach, post-bleach, and final images are displayed for reference. *Scale bar*, 5 μm. *D*, half-life values for myosin VI LI on clathrin-coated structures in HeLa cells ($t_{1/2} = 13 \pm 2$ s) and myosin VI NI on early endosomes in RPE cells ($t_{1/2} = 16 \pm 1$ s) are shown. The difference in values is not significant (unpaired *t* test, $n = 5$ sets of 5–9 cells for each construct; $p = 0.3$). *Error bars* represent S.E. *NS*, no significance. *E*, schematic shows domain structure of the eGFP-tagged myosin VI constructs used in this work. The wild type (WT) myosin VI LI and NI full-length constructs demonstrate that myosin VI consists of a motor domain (AA 1–759 of myosin VI), neck region, and IQ motif (AA 760–838 of myosin VI), proximal and medial tail domains (AA 839–980 of myosin VI), and a cargo-binding domain (AA 981–1285 of myosin VI). The following portions of this study utilize a tail construct of myosin VI (expressed from amino acid 839 to remove the motor domain/neck domain/IQ motif) and full-length, and tail forms of a myosin VI construct artificially dimerized by the inclusion of a leucine zipper region as an insert after amino acid 991 in the cargo-binding domain.

Clathrin proteins actively coat the endocytic vesicles and pits at the plasma membrane with which myosin VI LI associates, and their dynamic coating and uncoating behavior has been well characterized (34). Clathrin (($t_{1/2} = 28 \pm 3$ s) has a 2-fold longer half-life on clathrin-coated structures than myosin VI LI (($t_{1/2} = 13 \pm 2$ s) ($p = 0.001$) (Fig. 2, *B* and *C*).

Myosin VI LI Constructs Artificially Dimerized with a Leucine Zipper Turn Over on Clathrin-coated Structures with a 4-Fold Longer Half-life Than Wild Type Myosin VI LI—We next used our FRAP system for a systematic investigation of the functional behavior of myosin VI during endocytosis. To probe the fundamental question of whether myosin VI operates as a monomer or dimer in intracellular trafficking, we examined the turnover of a full-length, artificially dimerized construct of myosin VI relative to the wild type form. We modeled this artificial dimer construct on the myosin VI leucine zipper construct used in the majority of the *in vitro* biochemical studies of the properties of myosin VI (30, 35, 36). Our construct is dimerized with the same GCN4 leucine zipper sequence (32 AA) as the original construct, placed after the same amino acid

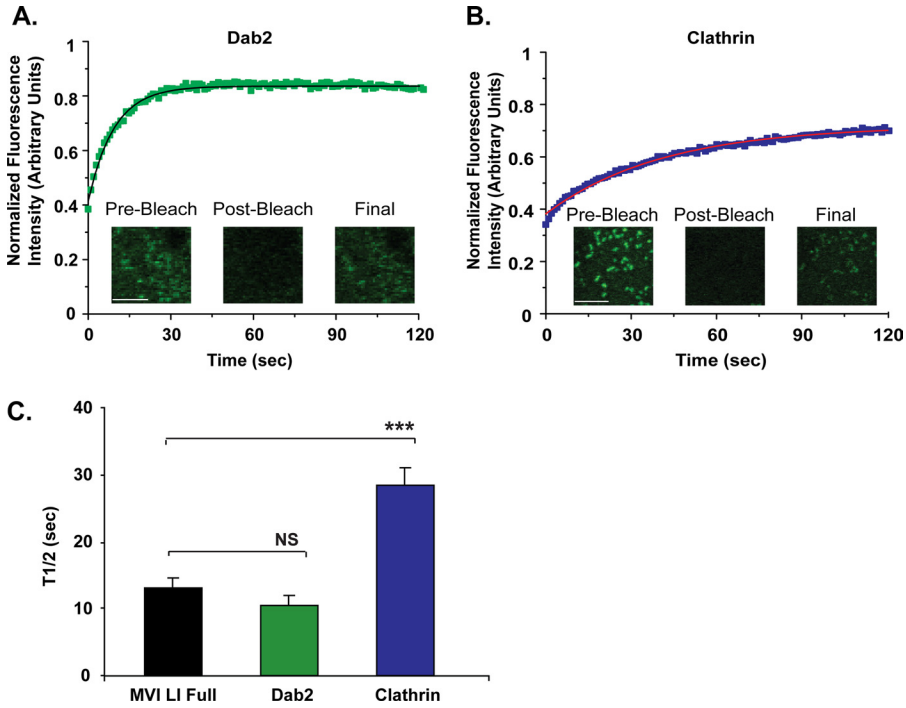

FIGURE 2. **Comparison with other members of the endocytic machinery.** *A* and *B*, FRAP of Dab2 (*A*) and clathrin constructs (*B*) on clathrin-coated structures in HeLa cells. Each *plot* represents an average of 1 data set (6 individual cells (Dab2) or 9 individual cells (clathrin) 0. The *solid line* in each *plot* represents a single exponential fit to the data ($R^2 = 0.98$ (*A*), 0.99 (*B*)). *Scale bar*, 5 μm. *C*, half-life values for Dab2 ($t_{1/2} = 10 \pm 1$ s) and clathrin ($t_{1/2} = 28 \pm 3$ s), in comparison with full-length myosin VI LI ($t_{1/2} = 13 \pm 2$ s). There is no significant difference in the half-life values for myosin VI LI and Dab2 (unpaired *t* test, $n = 5$ sets of 5–9 cells for each construct; $p = 0.2$). However, clathrin has a 2-fold longer half-life than myosin VI LI (unpaired *t* test, $n = 5$ sets of 5–10 cells for each construct; $p = 0.001$). *Error bars* represent S.E. *NS*, no significance. ***, $p \leq 0.001$.

in the tail region (human amino acid 991 of myosin VI) (Fig. 1*E*). Rather than truncating the construct after this leucine zipper like the original version, however, we have included the zipper as an insert in the full-length protein. This allows us to preserve the cargo-binding regions in the C-terminal tail domain necessary for association with adaptor proteins and lipids such as PIP_2 required for proper intracellular targeting and recruitment to endocytic structures. Like the eGFP-tagged wild type myosin VI construct, the leucine zipper construct is expressed at the C terminus of eGFP.

Because an artificially dimerized form of mammalian myosin VI has never before been viewed in live cells, we conducted an initial screen to assess its *in vivo* expression patterns, intracellular targeting, and suitability for our FRAP assay. The leucine zipper myosin VI LI construct shows a localization very similar to wild type myosin VI LI and similarly demonstrates noticeable targeting to punctate, clathrin-coated structures near the plasma membrane of HeLa cells fixed and labeled with antibodies to clathrin (Fig. 3*A*). To confirm the resulting implication that Dab2 binding is not impaired in the leucine zipper construct and that this construct is actively recruited to clathrin-coated structures via Dab2 binding, we used a mammalian two-hybrid assay to demonstrate that a leucine zipper myosin VI LI globular tail construct (AA 991–1317) binds to Dab2 *in vivo* (AA 550–770) in a manner similar to a wild type myosin VI LI globular tail construct (AA 1030–1285) ($p = 0.7$, supplemental Fig. 1). In comparison, *in vivo* Dab2 binding is completely abolished in a myosin VI LI globular tail construct containing a single point mutation in the Dab2-binding region of the tail (WWY→WLY, AA 1030–1285) (supplemental Fig. 1).

FRAP was then used to assess the turnover rate of the leucine zipper full-length myosin VI LI construct on clathrin-coated vesicles (Fig. 3*B*). This construct has a 4-fold longer half-life ($t_{1/2} = 48 \pm 8$ s) than wild type myosin VI ($t_{1/2} = 13 \pm 2$ s) ($p = 0.002$) (Fig. 3*C*).

Myosin VI LI Tail Construct Turns Over at the Same Rate as Full-length Myosin VI LI on Clathrin-coated Structures—To examine the relative importance of the myosin VI tail region in determining the dynamic interaction with membranes in the endocytic pathway, we compared the behavior of an eGFP-tagged tail construct of myosin VI LI on clathrin-coated structures with full-length myosin VI LI. This tail construct consists of the C-terminal portion of the protein (proximal and medial tail regions plus the cargo-binding domain), expressed from amino acid 839 of the full-length construct to exclude the motor, neck, and IQ motif present at the N terminus (Fig. 1*E*). Most importantly, this tail construct contains the binding domains for Dab2 and PIP_2 required for targeting to clathrin-coated structures at the plasma membrane.

The tail domain interacts dynamically with clathrin-coated structures with a half-life of 14 ± 1 s, which is similar to that found for full-length myosin VI ($t_{1/2} = 13 \pm 2$ s) ($p = 0.2$), suggesting that the tail region is the primary determinant of the interaction time (Fig. 4, *A* and *C*).

We also quantified the half-life of a dimeric tail construct containing a leucine zipper motif after the domain originally thought to be the coiled-coil-forming region (Fig. 1*E*). The half-life of this construct (49 ± 16 s) is similar to that found for the dimerized full-length construct (48 ± 8 s) ($p = 0.9$), again sug-

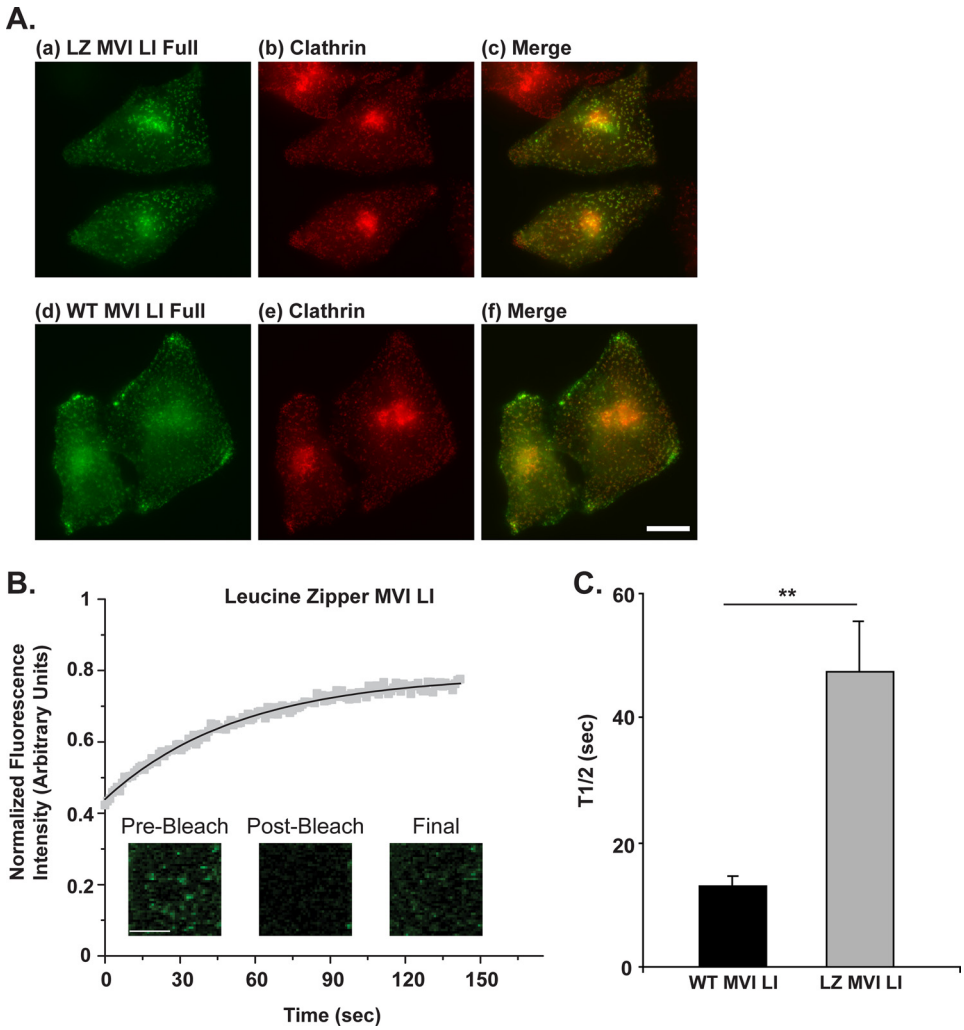

FIGURE 3. **Myosin VI LI constructs artificially dimerized with a leucine zipper turn over on clathrin-coated structures with a 4-fold longer half-life than wild type myosin VI LI.** *A*, *upper panel*, *a–c*, artificially dimerized myosin VI-eGFP (*a*) co-localized with endogenous clathrin (*b*) in HeLa cells. Cells were labeled by immunofluorescence with a polyclonal antibody to eGFP and a monoclonal antibody to clathrin. *Lower panel*, *d–f*, comparative depiction of the distribution of wild type myosin VI-eGFP (*d*) with respect to clathrin-coated structures (*e*). The similarity in the distribution patterns of the wild type and artificially dimerized forms is clearly visible. *Scale bar*, 10 μm. *B*, FRAP of myosin VI LI leucine zipper constructs on clathrin-coated structures in HeLa cells. The *plot* represents an average of 1 data set (9 individual cells). The *solid line* represents a single exponential fit to the data ($R^2 = 0.99$). *Scale bar*, 5 μm. *C*, leucine zipper myosin VI LI has a half-life on clathrin-coated structures ($t_{1/2} = 48 \pm 8$ s) that is 4-fold longer than wild type myosin VI LI ($t_{1/2} = 13 \pm 2$ s) (unpaired *t* test, $n = 4–5$ sets of 5–9 cells for each construct; $p = 0.002$). *Error bars* represent S.E. **, $p \leq 0.01$.

gesting that the tail region is of prime importance in determining these dynamics (Fig. 4, *B* and *D*).

Summary of Half-life and Percentage Recovery Values—For clarity, the half-life values of all constructs tested are summarized in Table 1. This table also displays the average percent recovery of each construct, a value representing the average percentage of initial fluorescence returning to a given bleached region with time. The average percent recovery of all constructs analyzed was comparable, with an overall average of 78.74 ± 0.02%. This recovery level falls within the range seen in other FRAP studies of proteins involved in the endocytic pathway (*e.g.* clathrin, actin) (37, 38).

DISCUSSION

We used a FRAP-based assay to examine the turnover and basic dynamics of myosin VI and its binding partner Dab2 on membrane structures in the endocytic pathway. The LI isoform of myosin VI has been shown to associate with clathrin-coated structures and to play a functional role in the early stages of the endocytic pathway (7, 9), whereas the NI isoform of myosin VI has been shown to have a functional role in association with early endosomes (11, 13). No studies, however, have examined the dynamics of the recruitment and life time of myosin VI on these endocytic structures or, in fact, on any intracellular structure. As such we use a FRAP microscopy assay in HeLa and RPE cells to demonstrate that myosin VI turns over dynamically on endocytic structures with a reproducible, characteristic half-life. This robust, characteristic half-life is consistent across multiple endocytic compartments (clathrin-coated structures *versus* early endosomes), across different myosin VI isoforms (no insert *versus* large insert isoforms), and across different cell lines (HeLa *versus* RPE cells). The same characteristic half-life is shared by the myosin VI-binding partner Dab2 known to recruit myosin VI to clathrin-coated pits and vesicles, a result that offers insight into the relative dynamic behavior of myosin proteins and their binding partners in general.

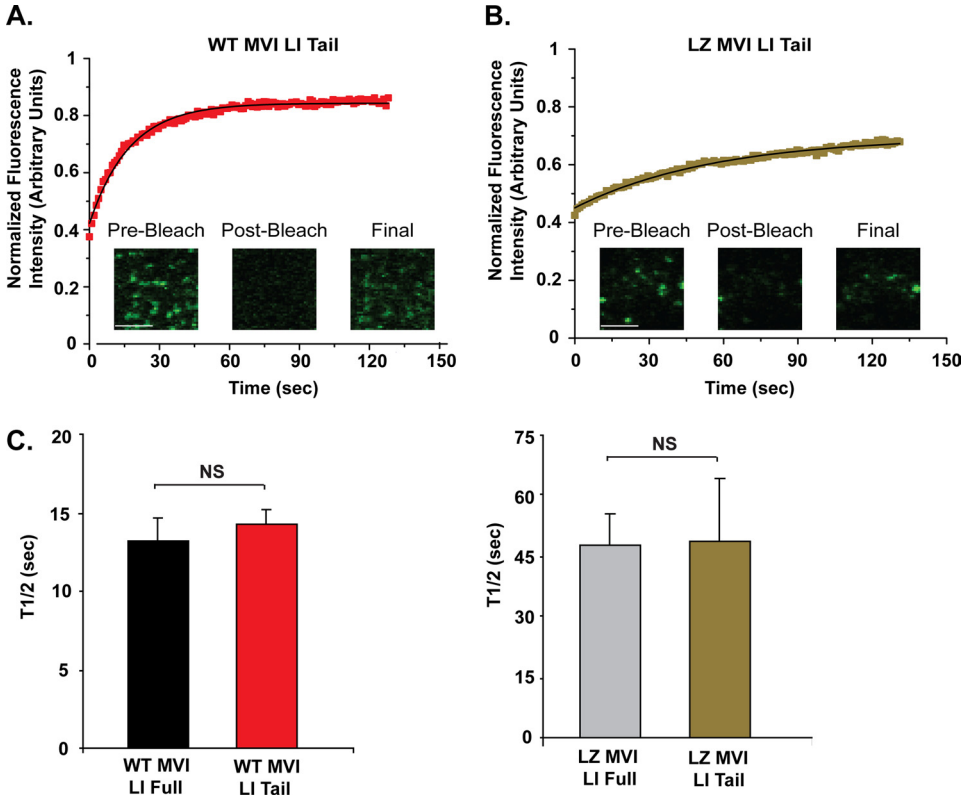

FIGURE 4. **Wild type and artificially dimerized myosin VI LI tail constructs turn over at the same rate as their full-length counterparts on clathrin-coated structures.** *A*, FRAP recovery curve for wild type myosin VI LI tail construct. This *plot* represents an average of 1 data set (8 individual cells). The *solid line* represents a single exponential fit to the data ($R^2 = 0.99$). *Scale bar*, 5 μm. *B*, FRAP of the leucine zipper myosin VI LI tail construct on clathrin-coated structures in HeLa cells. This *plot* represents an average of 1 data set (11 individual cells). The *solid line* represents a single exponential fit to the data ($R^2 = 0.99$). *Scale bar*, 5 μm. *C*, half-life value for the wild type myosin VI LI tail construct ($t_{1/2} = 14 \pm 1$ s), in comparison with full-length, wild type myosin VI LI ($t_{1/2} = 13 \pm 2$ s). There is no significant difference between these values ($p = 0.6$). *D*, half-life value for the leucine zipper myosin VI LI tail construct ($t_{1/2} = 49 \pm 16$ s), in comparison with full-length leucine zipper myosin VI LI ($t_{1/2} = 48 \pm 8$ s). There is no significant difference between these values (unpaired *t* test, $n = 4-6$ sets of 5–11 cells for each construct; $p = 0.9$). *Error bars* represent S.E. *NS*, no significance.

TABLE 1

Half-life and percentage recovery values

FRAP analysis values are displayed in the order in which they are presented under "Results." MVI, myosin VI; LI, large insert; LZ, leucine zipper; EE, early endosome; CCS, clathrin-coated structure.

Protein	Endocytic structure	Average half-life	Average recovery
		s	*%*
Wild type MVI NI full	EE	16 ± 1	84.27 ± 0.02
Wild type MVI LI full	CCS	13 ± 2	74.96 ± 0.02
Dab2	CCS	10 ± 1	84.53 ± 0.02
Clathrin	CCS	28 ± 3	76.71 ± 0.02
LZ MVI LI full	CCS	48 ± 8	77.48 ± 0.02
Wild type MVI LI tail	CCS	14 ± 1	83.332 ± 0.004
LZ MVI LI tail	CCS	49 ± 16	69.90 ± 0.02

Our demonstration that the turnover of the myosin VI LI isoform on clathrin-coated structures is 2-fold faster than the turnover of the associated clathrin coat protein offers insight into the basics of myosin VI function during the early stages of endocytosis. The more rapid exchange of myosin VI demonstrates that the motor is not likely to play a long term anchoring role on a given clathrin-coated structure, but instead may be involved in short term tethering or transport processes. These functional implications are reinforced when one compares the half-life of the large insert myosin VI isoform on clathrin-coated structures (13 ± 2 s) with the overall, average lifetime of a clathrin-coated vesicle (30–90 s) (39–41): it is clear from such a comparison that a given myosin VI LI protein remains only temporarily associated with a given clathrin-coated structure, rather than tethering a vesicle long term or stably binding to one vesicle for transport throughout its life cycle. This is in agreement with the proposed function for the myosin VI LI isoform, which localizes to the apical domain of the polarized epithelial cells in which it is expressed and has been suggested to transport transmembrane receptors from the tip to the base of a microvillus (21, 42). In this role, myosin VI moves and clusters plasma membrane proteins into a clathrin-coated pit, a function that requires only a transient association with clathrin-coated pits/vesicles. It is interesting to compare this short term functionality and relatively short half-life of myosin VI on the endocytic pathway with the more stable role and longer half-life of myosin II in stress fibers ($t_{1/2} = \sim$90 s, (43)).

Recruitment and Turnover of Myosin VI on CCSs—Our experiments provide further insight into the regions and domains of myosin VI that regulate dynamic recruitment and turnover on CCSs. Our previous work shows that the cargo-binding tail containing the Dab2-binding site appears to be sufficient to allow targeting of myosin VI to CCSs (32). The present demonstration that the turnover rate of the myosin VI tail on CCSs is the same as that of the full-length molecule agrees with these previous data and appears to imply that the motor domain with its ATPase- and actin-binding activities plays no part in myosin VI recruitment and turnover on these structures. How-

ever, the finding that the turnover rates of the tail and its binding partner Dab2 are the same offers a possible explanation: the adaptor protein Dab2 recruits myosin VI via its cargo-binding tail domain, and the resulting complex binds to CCSs via Dab2; when Dab2 is released, myosin VI is also released. In this scenario, a tail construct of myosin VI would reasonably share the same Dab2-based turnover dynamics as the full-length protein. This suggestion of a binding partner as the determinant of myosin VI turnover dynamics provides insight into the general interaction between myosin proteins and their binding partners.

Monomer/Dimer Nature of Myosin VI—The monomeric *versus* dimeric nature of myosin VI has been a fundamental question in the field for many years now. The original prediction of a coiled-coil α-helical region due to a repeating sequence in the myosin VI tail domain was viewed as an indication of the naturally dimeric nature of myosin VI (23). As such, the majority of the *in vitro* characterizations of myosin VI to date have been conducted using a truncated form of this protein artificially dimerized via the incorporation of a C-terminal leucine zipper after amino acid 992 in the porcine myosin VI tail domain. More recently, however, it was demonstrated that endogenous pools of myosin VI exist almost entirely in monomeric form when purified for *in vitro* studies (<1% are dimeric) and suggested that the central region of the myosin VI tail may form a single α-helical domain rather than a coiled-coil (24). Further studies have suggested that perhaps such natively monomeric myosin VI is selectively dimerized upon binding of cargo or other binding partners to form a transient, functionally dimeric state (44–46). Given these conflicting data, it has become increasingly essential to determine whether myosin VI operates solely as a dimer, operates solely as a monomer, or undergoes a functional transition between these states *in vivo*.

We therefore designed an artificially dimerized leucine zipper construct based upon the construct used in the majority of the *in vitro* studies of myosin VI (30, 35, 36) but possessing the unique capacity for live cell functional expression due to our inclusion of the critical targeting region (cargo-binding domain) in the tail domain. This construct allowed us to conduct a critical comparison of the functional behavior of wild type *versus* artificially dimerized myosin VI in the endocytic pathway *in vivo*. We demonstrate that an artificially dimerized form of myosin VI has a 4-fold longer half-life than wild type myosin VI during turnover on clathrin-coated structures. This suggests that native myosin VI does not function as a stable dimer on the endocytic pathway, but rather behaves functionally as a monomer or in a dynamic equilibrium between monomeric and dimeric states (*e.g.* in the type of binding partner-mediated monomer/dimer equilibrium suggested by Yu *et al.* (45)). This can be understood in terms of a Dab2-based regulation of myosin VI turnover dynamics if one considers that a given full-length or tail version of artificially dimerized myosin VI will necessarily bind to two distinct Dab2 proteins (one to each tail in the dimer). The half-life-defining release of an artificial dimer from a clathrin-coated structure will thus depend on the sequential release of these two distinct Dab2 proteins. The time required for full detachment by a doubly bound dimeric protein would therefore reasonably be longer than the time required for full release of a wild type myosin VI bound to a clathrin-coated structure solely as a monomer (via one Dab2 attachment site), bound in a wild type population including bound monomeric and dimeric proteins, or bound as a transiently dimeric protein that splits into individual monomers before dissociation. Thus, our results demonstrate that myosin VI does not function in the endocytic pathway as a preformed stable dimer. This important insight into the functional nature of myosin VI distinctly reduces the likelihood of one of the three considered options for myosin VI function (solely monomer, solely dimer, or a monomer/dimer equilibrium (47, 48)), narrowing future examinations of the functional behavior of myosin VI to a distinction between monomer and monomer/dimer states.

Acknowledgments—We thank C. Combs and D. Malide (NHLBI, National Institutes of Health Light Microscopy Core Facility) for assistance with microscopy and image analysis and M. Maciejewski (NHLBI) for advice on statistical analysis.

REFERENCES

1. Wells, A. L., Lin, A. W., Chen, L. Q., Safer, D., Cain, S. M., Hasson, T., Carragher, B. O., Milligan, R. A., and Sweeney, H. L. (1999) Myosin VI is an actin-based motor that moves backwards. *Nature* **401,** 505–508
2. Park, H., Li, A., Chen, L. Q., Houdusse, A., Selvin, P. R., and Sweeney, H. L. (2007) The unique insert at the end of the myosin VI motor is the sole determinant of directionality. *Proc. Natl. Acad. Sci. U.S.A.* **104,** 778–783
3. Warner, C. L., Stewart, A., Luzio, J. P., Steel, K. P., Libby, R. T., Kendrick-Jones, J., and Buss, F. (2003) Loss of myosin VI reduces secretion and the size of the Golgi in fibroblasts from Snell's waltzer mice. *EMBO J.* **22,** 569–579
4. Chibalina, M. V., Poliakov, A., Kendrick-Jones, J., and Buss, F. (2010) Myosin VI and optineurin are required for polarized EGFR delivery and directed migration. *Traffic* **11,** 1290–1303
5. Au, J. S., Puri, C., Ihrke, G., Kendrick-Jones, J., and Buss, F. (2007) Myosin VI is required for sorting of AP-1B-dependent cargo to the basolateral domain in polarized MDCK cells. *J. Cell Biol.* **177,** 103–114
6. Bond, L. M., Peden, A. A., Kendrick-Jones, J., Sellers, J. R., and Buss, F. (2011) Myosin VI and its binding partner optineurin are involved in secretory vesicle fusion at the plasma membrane. *Mol. Biol. Cell* **22,** 54–65
7. Buss, F., Arden, S. D., Lindsay, M., Luzio, J. P., and Kendrick-Jones, J. (2001) Myosin VI isoform localized to clathrin-coated vesicles with a role in clathrin-mediated endocytosis. *EMBO J.* **20,** 3676–3684
8. Taylor, M. J., Perrais, D., and Merrifield, C. J. (2011) A high precision survey of the molecular dynamics of mammalian clathrin-mediated endocytosis. *PLoS Biol.* **9,** e1000604
9. Ameen, N., and Apodaca, G. (2007) Defective CFTR apical endocytosis and enterocyte brush border in myosin VI-deficient mice. *Traffic* **8,** 998–1006
10. Osterweil, E., Wells, D. G., and Mooseker, M. S. (2005) A role for myosin VI in postsynaptic structure and glutamate receptor endocytosis. *J. Cell Biol.* **168,** 329–338
11. Aschenbrenner, L., Lee, T., and Hasson, T. (2003) Myo6 facilitates the translocation of endocytic vesicles from cell peripheries. *Mol. Biol. Cell* **14,** 2728–2743
12. Inoue, T., Kon, T., Ohkura, R., Yamakawa, H., Ohara, O., Yokota, J., and Sutoh, K. (2008) BREK/LMTK2 is a myosin VI-binding protein involved in endosomal membrane trafficking. *Genes Cells* **13,** 483–495
13. Chibalina, M. V., Seaman, M. N., Miller, C. C., Kendrick-Jones, J., and Buss, F. (2007) Myosin VI and its interacting protein LMTK2 regulate tubule formation and transport to the endocytic recycling compartment. *J. Cell Sci.* **120,** 4278–4288
14. Yoshida, H., Cheng, W., Hung, J., Montell, D., Geisbrecht, E., Rosen, D., Liu, J., and Naora, H. (2004) Lessons from border cell migration in the

Drosophila ovary: a role for myosin VI in dissemination of human ovarian cancer. *Proc. Natl. Acad. Sci. U.S.A.* **101,** 8144–8149
15. Dunn, T. A., Chen, S., Faith, D. A., Hicks, J. L., Platz, E. A., Chen, Y., Ewing, C. M., Sauvageot, J., Isaacs, W. B., De Marzo, A. M., and Luo, J. (2006) A novel role of myosin VI in human prostate cancer. *Am. J. Pathol.* **169,** 1843–1854
16. Mohiddin, S. A., Ahmed, Z. M., Griffith, A. J., Tripodi, D., Friedman, T. B., Fananapazir, L., and Morell, R. J. (2004) Novel association of hypertrophic cardiomyopathy, sensorineural deafness, and a mutation in unconventional myosin VI (*MYO6*). *J. Med. Genet.* **41,** 309–314
17. Melchionda, S., Ahituv, N., Bisceglia, L., Sobe, T., Glaser, F., Rabionet, R., Arbones, M. L., Notarangelo, A., Di Iorio, E., Carella, M., Zelante, L., Estivill, X., Avraham, K. B., and Gasparini, P. (2001) *MYO6*, the human homologue of the gene responsible for deafness in Snell's waltzer mice, is mutated in autosomal dominant nonsyndromic hearing loss. *Am. J. Hum. Genet.* **69,** 635–640
18. Ahmed, Z. M., Morell, R. J., Riazuddin, S., Gropman, A., Shaukat, S., Ahmad, M. M., Mohiddin, S. A., Fananapazir, L., Caruso, R. C., Husnain, T., Khan, S. N., Riazuddin, S., Griffith, A. J., Friedman, T. B., and Wilcox, E. R. (2003) Mutations of *MYO6* are associated with recessive deafness, DFNB37. *Am. J. Hum. Genet.* **72,** 1315–1322
19. Avraham, K. B., Hasson, T., Steel, K. P., Kingsley, D. M., Russell, L. B., Mooseker, M. S., Copeland, N. G., and Jenkins, N. A. (1995) The mouse Snell's waltzer deafness gene encodes an unconventional myosin required for structural integrity of inner ear hair cells. *Nat. Genet.* **11,** 369–375
20. Knudsen, B. (2006) Migrating with myosin VI. *Am. J. Pathol.* **169,** 1523–1526
21. Buss, F., Luzio, J. P., and Kendrick-Jones, J. (2001) Myosin VI, a new force in clathrin mediated endocytosis. *FEBS Lett.* **508,** 295–299
22. Hasson, T. (2003) Myosin VI: two distinct roles in endocytosis. *J. Cell Sci.* **116,** 3453–3461
23. Rock, R. S., Ramamurthy, B., Dunn, A. R., Beccafico, S., Rami, B. R., Morris, C., Spink, B. J., Franzini-Armstrong, C., Spudich, J. A., and Sweeney, H. L. (2005) A flexible domain is essential for the large step size and processivity of myosin VI. *Mol. Cell* **17,** 603–609
24. Lister, I., Schmitz, S., Walker, M., Trinick, J., Buss, F., Veigel, C., and Kendrick-Jones, J. (2004) A monomeric myosin VI with a large working stroke. *EMBO J.* **23,** 1729–1738
25. Umeki, N., Jung, H. S., Watanabe, S., Sakai, T., Li, X. D., Ikebe, R., Craig, R., and Ikebe, M. (2009) The tail binds to the head-neck domain, inhibiting ATPase activity of myosin VIIA. *Proc. Natl. Acad. Sci. U.S.A.* **106,** 8483–8488
26. Yang, Y., Baboolal, T. G., Siththanandan, V., Chen, M., Walker, M. L., Knight, P. J., Peckham, M., and Sellers, J. R. (2009) A FERM domain autoregulates *Drosophila* myosin 7a activity. *Proc. Natl. Acad. Sci. U.S.A.* **106,** 4189–4194
27. Buss, F., Spudich, G., and Kendrick-Jones, J. (2004) Myosin VI: cellular functions and motor properties. *Annu. Rev. Cell Dev. Biol.* **20,** 649–676
28. Spink, B. J., Sivaramakrishnan, S., Lipfert, J., Doniach, S., and Spudich, J. A. (2008) Long single α-helical tail domains bridge the gap between structure and function of myosin VI. *Nat. Struct. Mol. Biol.* **15,** 591–597
29. Trybus, K. M., Freyzon, Y., Faust, L. Z., and Sweeney, H. L. (1997) Spare the rod, spoil the regulation: necessity for a myosin rod. *Proc. Natl. Acad. Sci. U.S.A.* **94,** 48–52
30. Rock, R. S., Rice, S. E., Wells, A. L., Purcell, T. J., Spudich, J. A., and Sweeney, H. L. (2001) Myosin VI is a processive motor with a large step size. *Proc. Natl. Acad. Sci. U.S.A.* **98,** 13655–13659
31. Yeh, E., Haase, J., Paliulis, L. V., Joglekar, A., Bond, L., Bouck, D., Salmon, E. D., and Bloom, K. S. (2008) Pericentric chromatin is organized into an intramolecular loop in mitosis. *Curr. Biol.* **18,** 81–90
32. Spudich, G., Chibalina, M. V., Au, J. S., Arden, S. D., Buss, F., and Kendrick-Jones, J. (2007) Myosin VI targeting to clathrin-coated structures and dimerization is mediated by binding to Disabled-2 and PtdIns(4,5)P_2. *Nat. Cell Biol.* **9,** 176–183
33. Morris, S. M., Arden, S. D., Roberts, R. C., Kendrick-Jones, J., Cooper, J. A., Luzio, J. P., and Buss, F. (2002) Myosin VI binds to and localises with Dab2, potentially linking receptor-mediated endocytosis and the actin cytoskeleton. *Traffic* **3,** 331–341
34. Kirchhausen, T. (2000) Clathrin. *Annu. Rev. Biochem.* **69,** 699–727
35. Nishikawa, S., Homma, K., Komori, Y., Iwaki, M., Wazawa, T., Hikikoshi Iwane, A., Saito, J., Ikebe, R., Katayama, E., Yanagida, T., and Ikebe, M. (2002) Class VI myosin moves processively along actin filaments backward with large steps. *Biochem. Biophys. Res. Commun.* **290,** 311–317
36. Okten, Z., Churchman, L. S., Rock, R. S., and Spudich, J. A. (2004) Myosin VI walks hand-over-hand along actin. *Nat. Struct. Mol. Biol.* **11,** 884–887
37. Wu, X., Zhao, X., Baylor, L., Kaushal, S., Eisenberg, E., and Greene, L. E. (2001) Clathrin exchange during clathrin-mediated endocytosis. *J. Cell Biol.* **155,** 291–300
38. Murthy, K., and Wadsworth, P. (2005) Myosin-II-dependent localization and dynamics of F-actin during cytokinesis. *Curr. Biol.* **15,** 724–731
39. Saffarian, S., Cocucci, E., and Kirchhausen, T. (2009) Distinct dynamics of endocytic clathrin-coated pits and coated plaques. *PLoS Biol.* **7,** e1000191
40. Massol, R. H., Boll, W., Griffin, A. M., and Kirchhausen, T. (2006) A burst of auxilin recruitment determines the onset of clathrin-coated vesicle uncoating. *Proc. Natl. Acad. Sci. U.S.A.* **103,** 10265–10270
41. Ehrlich, M., Boll, W., Van Oijen, A., Hariharan, R., Chandran, K., Nibert, M. L., and Kirchhausen, T. (2004) Endocytosis by random initiation and stabilization of clathrin-coated pits. *Cell* **118,** 591–605
42. Biemesderfer, D., Mentone, S. A., Mooseker, M., and Hasson, T. (2002) Expression of myosin VI within the early endocytic pathway in adult and developing proximal tubules. *Am. J. Physiol. Renal Physiol.* **282,** F785–794
43. Kondo, T., Hamao, K., Kamijo, K., Kimura, H., Morita, M., Takahashi, M., and Hosoya, H. (2011) Enhancement of myosin II/actin turnover at the contractile ring induces slower furrowing in dividing HeLa cells. *Biochem. J.* **435,** 569–576
44. Park, H., Ramamurthy, B., Travaglia, M., Safer, D., Chen, L. Q., Franzini-Armstrong, C., Selvin, P. R., and Sweeney, H. L. (2006) Full-length myosin VI dimerizes and moves processively along actin filaments upon monomer clustering. *Mol. Cell* **21,** 331–336
45. Yu, C., Feng, W., Wei, Z., Miyanoiri, Y., Wen, W., Zhao, Y., and Zhang, M. (2009) Myosin VI undergoes cargo-mediated dimerization. *Cell* **138,** 537–548
46. Phichith, D., Travaglia, M., Yang, Z., Liu, X., Zong, A. B., Safer, D., and Sweeney, H. L. (2009) Cargo binding induces dimerization of myosin VI. *Proc. Natl. Acad. Sci. U.S.A.* **106,** 17320–17324
47. Spudich, J. A., and Sivaramakrishnan, S. (2010) Myosin VI: an innovative motor that challenged the swinging lever arm hypothesis. *Nat. Rev. Mol. Cell Biol.* **11,** 128–137
48. Buss, F., and Kendrick-Jones, J. (2008) How are the cellular functions of myosin VI regulated within the cell? *Biochem. Biophys. Res. Commun.* **369,** 165–175